

# The effect of a unique halide-stabilizing residue on the catalytic properties of haloalkane dehalogenase DatA from *Agrobacterium tumefaciens* C58

Khomaini Hasan<sup>1,\*</sup>, Artur Gora<sup>1,\*</sup>, Jan Brezovsky<sup>1</sup>, Radka Chaloupkova<sup>1</sup>, Hana Moskalikova<sup>1</sup>, Andrea Fortova<sup>1</sup>, Yuji Nagata<sup>2</sup>, Jiri Damborsky<sup>1</sup> and Zbynek Prokop<sup>1</sup>

<sup>1</sup> Loschmidt Laboratories, Department of Experimental Biology and Research Centre for Toxic Compounds in the Environment, Faculty of Science, Masaryk University, Brno, Czech Republic

<sup>2</sup> Department of Environmental Life Sciences, Graduate School of Life Sciences, Tohoku University, Sendai, Japan

## Keywords

catalytic mechanism; enzyme kinetics; halide-stabilizing residue; haloalkane dehalogenase; substrate specificity

## Correspondence

Z. Prokop, Loschmidt Laboratories, Department of Experimental Biology and Research Centre for Toxic Compounds in the Environment, Faculty of Science, Masaryk University, Kamenice 5/A13, 62500 Brno, Czech Republic  
Fax: +420 5 4949 6302  
Tel: +420 5 4949 6667  
E-mail: zbynek@chemi.muni.cz

\*These authors contributed equally to this work.

(Received 14 January 2013, revised 5 March 2013, accepted 6 March 2013)

doi:10.1111/febs.12238

Haloalkane dehalogenases catalyze the hydrolysis of carbon–halogen bonds in various chlorinated, brominated and iodinated compounds. These enzymes have a conserved pair of halide-stabilizing residues that are important in substrate binding and stabilization of the transition state and the halide ion product via hydrogen bonding. In all previously known haloalkane dehalogenases, these residues are either a pair of tryptophans or a tryptophan–asparagine pair. The newly-isolated haloalkane dehalogenase DatA from *Agrobacterium tumefaciens* C58 ([EC 3.8.1.5](#)) possesses a unique halide-stabilizing tyrosine residue, Y109, in place of the conventional tryptophan. A variant of DatA with the Y109W mutation was created and the effects of this mutation on the structure and catalytic properties of the enzyme were studied using spectroscopy and pre-steady-state kinetic experiments. Quantum mechanical and molecular dynamics calculations were used to obtain a detailed analysis of the hydrogen-bonding patterns within the active sites of the wild-type and the mutant, as well as of the stabilization of the ligands as the reaction proceeds. Fluorescence quenching experiments suggested that replacing the tyrosine with tryptophan improves halide binding by 3.7-fold, presumably as a result of the introduction of an additional hydrogen bond. Kinetic analysis revealed that the mutation affected the substrate specificity of the enzyme and reduced its  $K_{0.5}$  for selected halogenated substrates by a factor of 2–4, without impacting the rate-determining hydrolytic step. We conclude that DatA is the first natural haloalkane dehalogenase that stabilizes its substrate in the active site using only a single hydrogen bond, which is a new paradigm in catalysis by this enzyme family.

## Introduction

Haloalkane dehalogenases (HLDs) are bacterial enzymes that catalyze the hydrolytic dehalogenation of various halogenated compounds [1–3]. As a result of their broad specificity, HLDs have potential applica-

tions in biocatalysis, bioremediation and biosensing [4–8]. Structurally, the HLDs belong to the  $\alpha/\beta$  hydrolase superfamily. Their active site is deeply buried in the protein core, between the highly conserved  $\alpha/\beta$

## Abbreviations

HLD, haloalkane dehalogenase; MD, molecular dynamics; NAC, near attack configuration; PCA, principle component analysis; QM, quantum mechanics; SSG, substrate specificity group.

hydrolase fold main domain and a helical cap domain [4,9–19]. The key active site residues consist of a catalytic pentad: a nucleophile, a base, a catalytic acid and two halide-stabilizing residues. The dehalogenation reaction is initiated by the nucleophilic attack of an aspartic acid on the  $sp^3$ -hybridized carbon atom attached to the halogen. This breaks the carbon–halogen bond, forming a covalently bound alkyl–enzyme intermediate and a halide ion. The alkyl–enzyme intermediate is then hydrolyzed by a water molecule, which is activated by the catalytic base. The final reaction products are a halide ion, a proton and an alcohol [17–22].

Previous studies have demonstrated that the two halide-stabilizing residues in the active sites of HLDs are essential for their catalytic activity [23–26]. These residues hold the substrate in the configuration required for the  $S_N2$  reaction and then stabilize the reaction's transition state. They also stabilize the halide ion released during the cleavage of the carbon–halogen bond. These effects are exerted via a pair of hydrogen bonds, one donated by each of the two residues (Fig. 1A). The properties of the halide-stabilizing residues contribute significantly to the enzyme's stabilization efficiency [23]. The first halide-stabilizing residue is a highly conserved tryptophan located next to the nucleophile. Its other role is to maintain the nucleophile in the correct orientation for the nucleophilic attack [24]. The second halide-stabilizing residue is typically tryptophan or asparagine. Recently, a HLD named DatA was isolated from *Agrobacterium tumefaciens* C58 (EC 3.8.1.5) (newly *Agrobacterium fabrum* C58). Remarkably, this enzyme possesses a unique tyrosine residue in the position occupied by the (otherwise fully conserved) first halide-stabilizing tryptophan residue in other HLDs (Fig. 1B) [27,28].

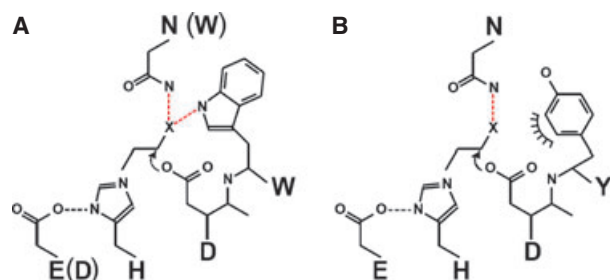


**Fig. 1.** The enzyme–substrate complex in a ‘conventional’ HLDs (A) and the DatA wild-type (B). The halide-stabilizing residues found in ‘conventional’ HLDs are either a tryptophan–tryptophan or a tryptophan–asparagine pair. The halide-stabilizing residues of DatA are a tyrosine–asparagine pair. Hydrogen bonds are indicated by dashed lines and hydrophobic contacts are indicated by an arc with spokes radiating towards the ligand.

In the present study, we report the results of an experimental and computational investigation into the impact of this unique halide-stabilizing residue on the catalytic properties of DatA. The mutant DatA01, which carries the substitution Y109W, was created by site-directed mutagenesis and then biochemically characterized and compared with the wild-type enzyme. Spectroscopic analyses, as well as steady-state and transient kinetic experiments, provided insights into the effects of the halide-stabilizing residues on halide-binding, substrate specificity and reaction kinetics. Quantum mechanics (QM) calculations and molecular dynamics (MD) simulations were performed to complement the experimental studies by providing information on how the active site residues interact with the substrate and the products formed during the reaction.

## Results

### Structural and thermostability analysis

The mutant protein Y109W was constructed by site-directed mutagenesis, expressed in *Escherichia coli* and purified to homogeneity using the two-step purification protocol [28]. The correct folding of the purified mutant DatA01 was verified by CD spectroscopy. The far-UV CD spectrum of the native enzyme exhibited two negative features at 208 and 222 nm, which is typical of  $\alpha$ -helical content (Fig. S1). The spectrum of DatA01 was similar to that of the wild-type enzyme, indicating that the replacement of the tyrosine with the otherwise-conserved tryptophan had no effect on the overall secondary structure of the enzyme. The melting temperatures determined for DatA (48.3 °C) and DatA01 (51.8 °C) differed by 3.5 °C. The increased thermostability of DatA01 could be attributed to the replacement of tyrosine with the larger tryptophan, which strengthened the hydrophobic packing of the structure and improved the van der Waals contacts between the amino acid residues in the protein core [29].

### Substrate specificity analysis

Substrate specificity measured with 30 different halogenated substrates revealed different patterns for DatA and DatA01 (Fig. 2). The specific activity of DatA01 towards most of the tested substrates was lower than that of DatA. Interestingly, DatA01 showed increased specific activities towards several substrates: bis(2-chloroethyl)ether, 3-chloro-2-methylpropene, 1,2-dibromoethane, 1,2-dibromopropane, 1,2,3-tribromopropane, 1-bromo-2-chloroethane, 1,2-dibromo-3-chloropropane or 4-bromobutyronitrile.

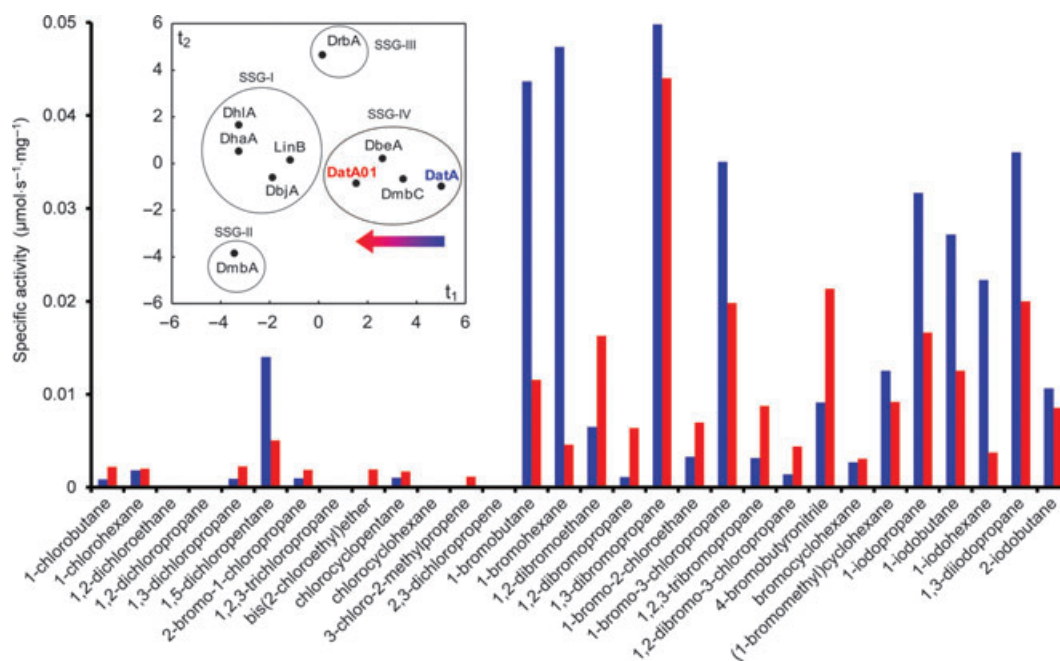


**Fig. 2.** Comparison of the substrate specificity profiles of DatA wild-type (blue) and DatA01 (red) for 30 different substrates. The insert shows the clustering of DatA, DatA01 and other characterized HLDs based on their activity towards the tested substrates. The  $t_1/t_2$  score plot obtained by principal component analysis explains 31% of the variance in the original dataset.

Changes in the substrate specificity were explored by principal component analysis (PCA). Although DatA01 and DatA were in the same substrate specificity group (SSG)-IV, the substitution of tyrosine for tryptophan significantly modulated the enzyme's substrate specificity, as indicated by the very different positions of the two enzymes on the scores plot (Fig. 2).

### Halide-binding analysis

The steady-state fluorescence of DatA and DatA01 was measured after mixing with different bromide concentrations (0–1500 mM). The intensity of fluorescence was recorded upon excitation at 280 nm for both tryptophan and tyrosine and selective excitation at 295 nm for tryptophan exclusively (Fig. 3). The fluorescence profile of the DatA wild-type upon excitation at 295 nm indicated only nonspecific fluorescence quenching as the bromide concentration increased, reflecting the effect of the anion as a general fluorescence quencher. By contrast, strong additional quenching was observed for the variant DatA01, suggesting the existence of a specific interaction between the bromide ion and the introduced tryptophan residue. The equilibrium constants for bromide binding ( $K_d$ ) in DatA and DatA01 were

determined based on fluorescence measurements upon excitation at 280 nm. The equilibrium dissociation constant for the mutant DatA01 ( $K_d = 34 \pm 4$  mM) was 3.7-fold lower than that for the wild-type DatA ( $K_d = 127 \pm 32$  mM). The replacement of the tyrosine with tryptophan thus stabilized the enzyme–halide complex.

### Steady-state kinetics

The kinetic constants determined for the wild-type DatA and the mutant DatA01 under steady-state conditions are summarized in Table 1. Both the wild-type and the mutant yielded hyperbolic kinetic profiles for their reactions with 1,3-dibromopropane and 1-bromohexane, suggesting classical Michaelis–Menten kinetics (data not shown). The sigmoidal profiles obtained in experiments using 1,3-diiodopropane, 1-chlorohexane and 1-bromobutane indicate that these substrates are hydrolyzed via a cooperative Hill mechanism. Regardless of the kinetic mechanism in operation or the substrate used, the  $K_{0.5}$  values for DatA01 were lower than those for the wild-type DatA. In particular, the  $K_{0.5}$  values for brominated substrates with DatA01 were 2.5–4.5-fold lower than those obtained with DatA, indicating that the mutant has a higher affinity for these substrates (Table 1). These data are

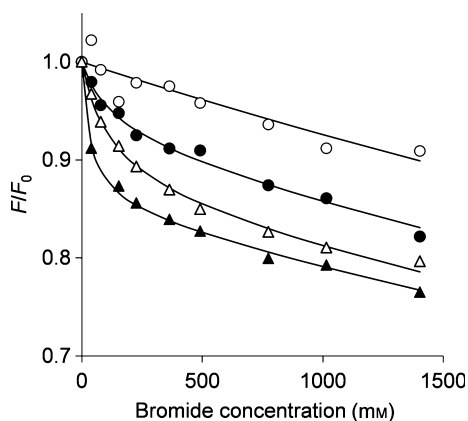


**Fig. 3.** Steady-state fluorescence of DatA (circle) and DatA01 (triangle) at different bromide concentrations (0–1500 mM). The fluorescence intensity was measured under excitation at 280 nm for DatA (●) and DatA01 (▲) and at 295 nm for DatA (○) and DatA01 (Δ). All measurements were conducted in 100 mM glycine buffer (pH 8.6) at room temperature in triplicate. Solid lines represent the best fits to the data based on the Stern-Volmer equation,  $F/F_0 = [1 + (f \cdot K_Q[X])]/(1 + K_{Br}[X])$ , in which  $F/F_0$  is the relative fluorescence,  $f$  is the relative fluorescence intensity of the enzyme–halide complex, and  $K_{Br}$  is the association equilibrium constant for the specific binding of bromide.  $K_Q$  is the quenching constant, which is the apparent association equilibrium constant for the nonspecific quenching interaction between bromide and the fluorophore.

consistent with the halide-binding results obtained from the fluorescence spectroscopy experiments, which indicated that tryptophan was a better halide-stabilizing residue than tyrosine. Moreover, substrate inhibition by 1-bromohexane (which suggests strong binding of multiple substrate molecules to the enzyme) was observed for DatA01 but not for the wild-type DatA. The catalytic rates of DatA01 were 2–6-fold lower than those of the wild-type for all of the tested substrates other than 1,3-dibromopropane and 1-chlorohexane. This reduction in  $k_{cat}$  is consis-

tent with the reduced specific activity observed as a result of the mutation (Fig. 2).

### Pre-steady-state kinetics

Transient kinetic analysis was used to obtain more information on the kinetics of the DatA and DatA01 catalytic cycles and their limiting factors. The pre-steady-state burst kinetics for 1-bromobutane hydrolysis were analyzed by the rapid quench flow technique. Clear pre-steady-state bursts were observed for substrate depletion and the corresponding formation of bromide ions with both DatA and DatA01, although no burst in alcohol formation was observed with either enzyme (Fig. 4). This indicates that substrate binding and the cleavage of the carbon–halogen bond are fast steps, and that hydrolysis of the alkyl–enzyme intermediate is the rate-determining step in the conversion of 1-bromobutane by both enzymes. Rate constants of  $2.6 \pm 0.2 \text{ s}^{-1}$  and  $1.2 \pm 0.1 \text{ s}^{-1}$  were obtained for DatA and DatA01, respectively, in the linear steady-state phase; the corresponding steady-state turnover numbers were  $1.5 \pm 0.01 \text{ s}^{-1}$  and  $0.7 \pm 0.02 \text{ s}^{-1}$  (Table 1). The calculated rates of halide formation during the burst phase for DatA and DatA01 were  $117 \pm 64 \text{ s}^{-1}$  and  $147 \pm 20 \text{ s}^{-1}$ , respectively. The higher burst rate for DatA01 indicates that it is more proficient than the wild-type at promoting the first step of the reaction (i.e. the cleavage of the carbon–halogen bond). The overall effect on Michaelis constant observed after the mutation is most likely associated with both increased rate of carbon–halogen bond cleavage and better stabilization of the enzyme–substrate complex. It has been suggested previously that the rate of carbon–halogen bond cleavage and the second-order dissociation constant for the enzyme and substrate complex are the main determinants of the Michaelis constant in HLDs [22].

**Table 1.** Steady-state kinetic parameters for DatA and DatA01 with seven different substrates determined at 37 °C in 100 mM glycine buffer (pH 8.6). The kinetic data were fitted to the Hill equation,  $v = k_{cat} \cdot S^n / (K_{0.5}^n + S^n)$ , where  $n$  is the Hill cooperativity coefficient and  $K_{0.5}$  is the half-maximal activity constant. The kinetic data for DatA were taken from Hasan *et al.* [28], with the exception of those for the substrate 1-bromobutane. ND, not determined.

Substrate	DatA				DatA01			
	$K_{0.5}$ (mM)	$k_{cat}$ ( $\text{s}^{-1}$ )	$n$	$K_{si}$ (mM)	$K_{0.5}$ (mM)	$k_{cat}$ ( $\text{s}^{-1}$ )	$n$	$K_{si}$ (mM)
1,3-Dibromopropane	$2.2 \pm 0.3$	$1.5 \pm 0.1$	1.0	ND	$0.82 \pm 0.08$	$1.3 \pm 0.1$	1.0	ND
1,3-Dichloropropane	> 4	> 0.01	1.0	ND	> 4	> 0.012	1.0	ND
1,3-Diiodopropane	$0.20 \pm 0.03$	$1.2 \pm 0.1$	$3.5 \pm 1.6$	ND	$0.16 \pm 0.02$	$0.72 \pm 0.02$	$2.7 \pm 0.8$	ND
1-Bromohexane	$0.14 \pm 0.09$	$1.7 \pm 0.1$	1.0	ND	$0.03 \pm 0.01$	$0.46 \pm 0.07$	1.0	$0.25 \pm 0.01$
1-Chlorohexane	$0.07 \pm 0.02$	$0.04 \pm 0.01$	$1.3 \pm 0.2$	ND	$0.06 \pm 0.01$	$0.04 \pm 0.01$	$2.2 \pm 0.6$	ND
1-Bromobutane	$0.53 \pm 0.01$	$1.5 \pm 0.1$	$1.7 \pm 0.1$	ND	$0.18 \pm 0.01$	$0.71 \pm 0.03$	$2.6 \pm 0.1$	ND

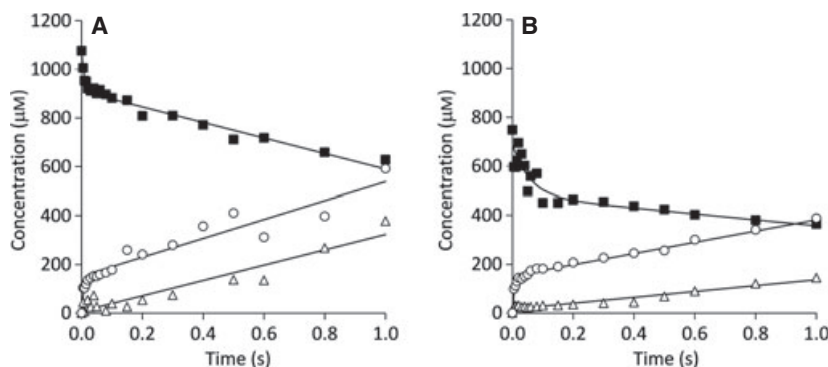


**Fig. 4.** Pre-steady-state burst of 1-bromobutane conversion by the haloalkane dehalogenases DatA (A) and DatA01 (B). Both reactions were performed in 100 mM glycine buffer (pH 8.6) at 37 °C. The concentrations of 1-bromobutane (■) and 1-butanol (Δ) were determined by GC and the bromide (○) concentration was analyzed by ion chromatography. Solid lines represent the best fit of the kinetic data to a linear equation for the alcohol product and to the burst equation,  $c = A_0[1 - \exp(-k_1 t)] + k_2 t$ , for the substrate and halide, where  $c$  is the concentration,  $A_0$  is the burst amplitude,  $t$  is the time, and  $k_1$  and  $k_2$  are rate constants.

### Molecular modelling

The docked poses of enzyme–substrate complexes were searched for geometries close to the near attack configuration (NAC) [30], in which the distance between the OD1 atom of the D108 residue and the carbon atom attached to the halogen is  $< 3.4$  Å and the angle between the halide, the carbon atom attached to the halide and the OD1 atom of D108 is between  $157^\circ$  and  $180^\circ$ . All of the chosen geometries fulfilled the NAC distance requirement; their NAC angles ranged from  $105^\circ$  to  $163^\circ$ . The geometries selected for further QM calculations are summarized in Table S1.

QM calculations were performed to investigate the effect of mutating the halogen-stabilizing residue on the rate of the  $S_N2$  reaction. A comparison of the calculated reaction profiles showed that the mutation of the halide-stabilizing residue reduced the activation energy for both brominated and iodinated compounds (Fig. S2 and Table S2). The activation energies calculated for chlorinated substrates were almost equal for both enzymes. The main interactions that stabilized the halogen atoms of the substrates were provided by residues H41, N43, P44, D108, Y109/W109, E127, F147, F160, G207, P208 and L211 (Fig. S3). The Y109 residue present in the wild-type enzyme provided less effective stabilization than the W109 residue in the mutant. Unexpectedly, inspection of the geometries during  $S_N2$  reaction revealed that the substrate's halogen atom was stabilized by only one hydrogen bond (donated by N43) in the wild-type enzyme, DatA. The second bond that is observed in other dehalogenases was not detected in the wild-type enzyme but was present in the mutant DatA01.

MD simulations of the complexes formed by DatA and DatA01 with 1-bromohexane were performed to

confirm the difference in stabilization. In DatA01, the halogen atom is stabilized by two hydrogen bonds; the average distance between the N43:2HD2 atom and the bromine atom is  $3.0 \pm 0.6$  Å, whereas that between the W109:HE1 atom and the bromine atom is  $2.8 \pm 0.4$  Å. By contrast, only N43 formed a hydrogen bond with the bromine atom in DatA, with an average length of  $2.9 \pm 0.5$  Å. The average distance between Y109:HH1 and the bromine atom is  $4.6 \pm 0.4$  Å, which is considerably longer than would be expected for a hydrogen bond (Fig. 5).

### Discussion

The haloalkane dehalogenase DatA from *A. tumefaciens* C58 is a recently discovered member of the versatile HLD family [28]. A sequence alignment of DatA with known HLDs revealed that DatA carries a unique tyrosine residue in the position commonly occupied by a tryptophan residue situated in close proximity to the nucleophile and is highly conserved in other members of the family. This residue has previously been shown to be important in stabilizing: (a) the binding of the substrate molecule in the enzyme–substrate, (b) the transition state of the  $S_N2$  reaction, and (c) the halide ion released after carbon–halogen bond cleavage [23]. We constructed a variant of this enzyme, DatA01, in which the tyrosine residue is replaced with tryptophan with the aim of studying the mutation's effect on the enzyme's structure and catalytic properties.

The quenching of the intrinsic fluorescence of HLDs upon halide binding has been reported previously [19,24–26] and was used to obtain quantitative information on how the mutation affected halide binding.

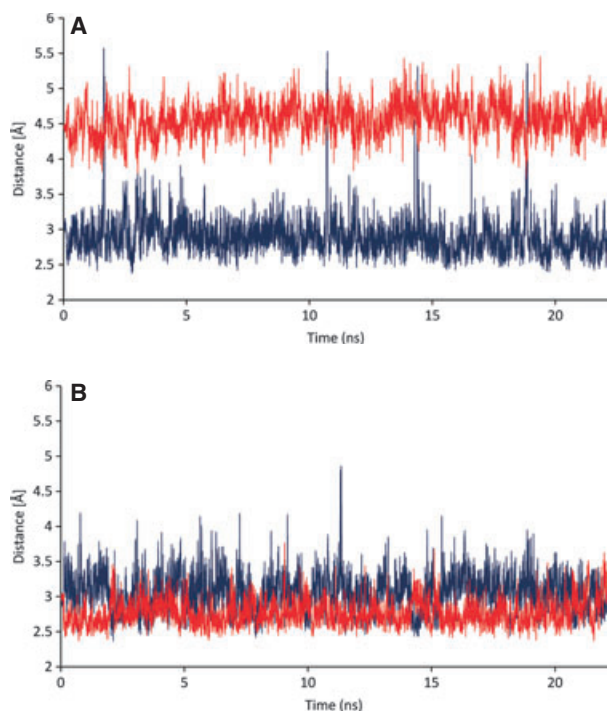


**Fig. 5.** Comparison of the distances between the bromide ion and the halide-stabilizing residues during MD simulations of (A) DatA and (B) DatA01 complexes with 1-bromohexane. Lines correspond to the moving average calculated over a moving ten-point frame. Red lines represent the distance W109:HE1–Br (DatA) or Y109:HH1–Br (DatA01); blue lines represent the distance N43:2HD2–Br.

The tryptophan-selective fluorescence spectrum of DatA01 confirmed that the introduced residue interacts specifically with the halide ion during bromide binding. Furthermore, the substitution of tyrosine by tryptophan significantly decreased the enzyme's equilibrium dissociation constant: the affinity of the DatA01 variant for bromide is 3.7-fold higher than that of the wild-type enzyme. The results from the halide binding experiments were consistent with those obtained in steady-state kinetics studies, in which the Y109W substitution reduced the enzyme's  $K_{0.5}$  values for all tested substrates. This suggests that the introduced tryptophan residue increases the mutant enzyme's affinity for the alkyl halide substrate, as well as the halide ion product of the hydrolysis reaction. In agreement with this finding, it has been previously reported that tryptophan is a more effective stabilizing residue than tyrosine [23–26]. The catalytic role of the tryptophan residues Trp125 and Trp175 forming the halide-binding site in the active site cavity of HLD DhlA has been studied by replacing these two residues by phenylalanine, arginine, tyrosine and glutamine [24]. The properties of these mutants indicated that the

interactions of Trp125 and Trp175 with the halogen atom of the substrate are essential for the cleavage of carbon–halogen bond. Most of these mutants show dramatically reduced catalytic performance. Unexpectedly, changing the tryptophan to tyrosine resulted in preservation of turnover number but increased the Michaelis constant [24]. The W175Y substitution in DhlA yielded a mutant with a lower binding affinity as a result of reduced rates of substrate binding and cleavage of the carbon–halogen bond. Furthermore, the W175Y substitution increased the rate of bromide release and the hydrolysis of alkyl–enzyme intermediate became the rate determining step for the mutant [26]. Transient kinetic analysis of DatA and DatA01 indicated that the Y109W mutation enhanced the stability of the enzyme–substrate complex and increased the rate of the carbon–halogen bond cleavage, although it did not result in change of rate-limiting step.

The computational analysis of the contribution of active site residues towards ligand stabilization indicated that the N43–W109 pair of the DatA01 mutant provides better stabilization of the halogen atom than the N43–Y109 pair of the DatA wild-type. Clearly, the hydrogens located on the aromatic ring of the tyrosine residue provide very little stabilization to the halogen atom. The geometric parameters obtained during QM calculations of the  $S_N2$  reaction and 20-ns MD simulations of the protein–substrate complex revealed that tyrosine cannot act as a hydrogen bond donor to stabilize the halogen atom/halide ion as the reaction proceeds. However, when it is replaced by a tryptophan residue, the new hydrogen bond is introduced (Fig. 5).

DatA01 was less active than the wild-type DatA towards most of the tested substrates. Semi-empirical QM calculations indicated that the Y109W mutation in DatA01 introduces the second hydrogen bond, which helps to stabilize the partial negative charge that develops on the halide ion as the carbon–bromine bond breaks (Fig. 5). This decreases the activation energy and enthalpy of the first step of the reaction. However, this beneficial effect on the  $S_N2$  step is counteracted by the mutation's negative effect on the rate-limiting step, namely the hydrolysis of the alkyl–enzyme intermediate in both DatA and DatA01 when using 1-bromobutane as the substrate. This observation explains why DatA can tolerate the 'loss' of a halide-stabilizing residue without compromising its catalytic activity towards the majority of tested halogenated substrates. The hydrolysis of the alkyl–enzyme intermediate has been previously identified as the rate-limiting step for LinB when using 1-chlorohexane,

chlorocyclohexane and bromocyclohexane as substrates [22]. Based on the fact that the substitution of the unique tyrosine for conserved tryptophan did not dramatically improve the catalytic activity, we speculate that *datA* is not a cryptic gene and that DatA is fully functional enzyme.

Interestingly, DatA01 exhibited improved activity towards several 1,2-dihalogenated substrates, comprising an important group of halogenated chemicals that are commonly used in industry and agriculture and also occur naturally. We speculate that the S<sub>N</sub>2 reaction may be the rate-limiting step for 1,2-dihalogenated substrates as a result of the steric hindrance of the attacking nucleophile arising from the presence of a second bulky halogen in the wild-type DatA.

Both DatA and DatA01 belong to the SSG-IV group of HLDs [31] and so the Y109W mutation did not cause a change in overall substrate specificity. However, the relative positions of DatA and DatA01 within the group are different and the addition of a second halide-stabilizing residue in close proximity to the nucleophile clearly affects the substrate specificity of DatA. The nature of the halide-stabilizing residues clearly has a strong effect on substrate specificity in this enzyme family.

In summary, the results of the present study demonstrate that the novel HLD DatA from *A. tumefaciens* C58 catalyses the hydrolytic dehalogenation of halogenated compounds using a single hydrogen bond to stabilize the halogenated substrate, the transition state of S<sub>N</sub>2 reaction and the halide product. This has not been observed with any other native HLD, demonstrating that DatA is the first representative of a new paradigm for catalysis by this versatile enzyme family.

## Experimental procedures

### Mutagenesis and protein purification

Established methods were used for digestion of plasmid DNA and PCR-amplified DNA fragments using restriction endonucleases, agarose gel electrophoresis and transformation into *E. coli* cells. Plasmid dsDNA was isolated using the GeneJET Plasmid Miniprep Kit (Fermentas, Burlington, Canada). The *datA01* gene that codes for the Y109W mutant was constructed by inverse PCR using the primers *datA01*-f: 5'-GTGCTGCAGGATTGGGGCGCGCGTTTT G-3' and *datA01*-r: 5'-CAAACGCCGCGCCCAATCCTGCAGCAC-3' (substitution underlined) in conjunction with the *Pfu* high-fidelity polymerase (Stratagene, La Jolla, CA, USA) in accordance with the manufacturer's instructions. A codon-optimized synthetic *datA* gene embedded in the cloning vector pUC18 was used as a template. The

*DpnI*-treated PCR product was transformed into *E. coli* DH5 $\alpha$  and the *datA01* gene was subcloned into expression vector pET21b between the *NdeI* and *HindIII* restriction sites. The expression and purification of DatA and DatA01 were carried out as reported previously [28].

### CD spectroscopy

CD spectra were recorded at room temperature (22 °C) using a Jasco J-810 spectropolarimeter (Jasco, Tokyo, Japan). Data were collected from 185 to 260 nm (scanning speed of 100 nm·min<sup>-1</sup>; response time of 1 s; bandwidth of 2 nm). The spectra were acquired with a cuvette path length of 0.1 cm and a protein concentration of 0.23 mg·mL<sup>-1</sup>. Each spectrum shown is the average of ten individual scans and was corrected for baseline noise. CD data were expressed in terms of the mean residue ellipticity ( $\Theta_{\text{MRE}}$ ) using the equation:

$$\Theta_{\text{MRE}} = \frac{\Theta_{\text{obs}} \cdot M_w \cdot 100}{n \cdot c \cdot l}$$

where  $\Theta_{\text{obs}}$  is the observed ellipticity in degrees,  $M_w$  is the protein molecular weight,  $n$  is number of residues,  $l$  is the cell path length,  $c$  is the protein concentration, and the factor 100 originates from the conversion of the molecular weight to mg·dmol<sup>-1</sup>.

The thermal stability of DatA and DatA01 was measured by heating a solution of the protein from 22 to 80 °C at 1 °C·min<sup>-1</sup>. The recorded thermal denaturation curves were approximately normalized to represent signal changes between ~1 and 0, and fitted to sigmoidal curves using ORIGIN, version 6.1 (OriginLab, Northampton, MA, USA). Melting temperatures ( $T_m$ ) were recorded as the midpoints of the normalized thermal transition for each protein.

### Substrate specificity profiles

The enzymes' substrate specificity was measured in 100 mM glycine buffer (pH 8.6) at 37 °C using a set of 30 different halogenated compounds, as reported previously [28]. The release of halide ions in each reaction was quantified by the method of Iwasaki *et al.* [32]. The matrix containing the specific activity data for DatA, DatA01 and eight well-characterized wild-type HLDs towards the 30 substrates was analyzed by PCA as described previously [31].

### Fluorescence spectroscopy

Steady-state fluorescence was measured in 1-cm quartz cuvettes using a Fluoromax-4P (Horiba Jobin Yvon, Edison, NJ, USA) fluorescence spectrometer. Fluorescence intensity was recorded at the emission maximum (334 nm) in response to the excitation of both tryptophan and tyrosine at 280 nm and to the selective excitation of tryptophan

at 295 nm. The fluorescence of wild-type DatA and DatA01 was recorded at different bromide concentrations ranging from 0 to 1500 mM. All fluorescence spectroscopy experiments were performed in 100 mM glycine buffer (pH 8.6) at 20 °C.

### Steady-state kinetics analysis

Steady-state kinetics experiments were performed using seven different substrates in 100 mM glycine buffer (pH 8.6) at 37 °C. After the addition of the substrate, the reaction mixture was pre-incubated for 30 min at 37 °C before initiating the reaction. The pre-incubated substrate (1 mL) was withdrawn and mixed with methanol containing 1,2-dichloroethane as an internal standard for quantification of the initial substrate concentration. The substrate concentration was quantified by GC-MS using a Trace 2000 instrument (Thermo Fisher Scientific, Waltham, MA, USA). The enzymatic reaction was initiated by adding an enzyme solution. The reaction's progress was monitored every 10 min and the rate of halide ion formation was quantified by the method of Iwasaki *et al.* [32]. The kinetic data were fitted by nonlinear regression using ORIGIN, version 6.1 (Origin Lab).

### Pre-steady-state kinetic analysis

Rapid quench-flow experiments were performed at 37 °C in a 100 mM glycine buffer (pH 8.6) using a QFM 400 rapid quench flow instrument (BioLogic, Grenoble, France). The reaction was started by rapidly mixing 70 µL of enzyme solution with 70 µL of substrate solution, and quenched with 100 µL of 0.8 M H<sub>2</sub>SO<sub>4</sub> after time intervals ranging from 2 ms to 1.6 s. The quenched mixture was directly injected into 0.5 mL of ice-cold diethyl ether containing 1,2-dichloroethane as an internal standard. After extraction, the diethyl ether layer containing the noncovalently bound substrate and the alcohol product was collected, dried on a short column containing anhydrous Na<sub>2</sub>SO<sub>4</sub>, and analyzed by GC-MS using a Trace 2000 instrument (Thermo Fisher Scientific, Waltham, MA, USA) and a DB-5MS capillary column (Agilent Technologies, Santa Clara, CA, USA). The bromide ion content of the water phase was measured using an 861 Advanced Compact IC ion chromatograph equipped with a METROSEP A Supp 5 column (Metrohm, Herisau, Switzerland).

### PCA

PCA was performed using STATISTICA, version 10.0 (StatSoft, Tulsa, OK, USA). The raw data were log-transformed and weighted relative to the individual enzyme's activity towards other substrates before analysis. Each specific activity value was incremented by 1 unit to avoid logarithmic transformation of zero values; the log of this new value

was taken and divided by the sum of all the log values for that particular enzyme. The log-transformed, weighted measure of that enzyme's activity towards that specific substrate (relative to its activity towards all of the other substrates) was thus obtained. Such transformed data were used to compare the specificity profile of DatA01 with previously defined SSGs of HLDs [31], without regard to overall specific activity.

### Molecular docking

The crystal structures of DatA and DatA01 were taken as starting points for modelling. Atoms with multiple alternative crystallographic positions were modelled in the alternate conformation A. All crystallographic water molecules and ions were removed. The polar hydrogens were added at a simulated pH of 8.5 using the H++ server [33]. Six substrates (1,3-dibromopropane, 1,3-dichloropropane, 1,3-diiodopropane, 1-bromoethane, 1-chlorohexane and 1-iodohexane) were docked into the DatA and DatA01 structures using AUTODOCK, version 4.0 [34]. This set of compounds was selected to permit comparisons of the effects of substrate size and the identity of the halide ion on the substrate's binding geometry. Gasteiger partial atomic charges, AUTODOCK atom types and solvation parameters were assigned to the ligands and the enzymes; nonpolar hydrogens and their charges were merged with their parent carbon atoms using MGL TOOLS [35]. A grid box of 64 × 64 × 64 points in the *x*, *y* and *z* dimensions was used with a grid spacing of 0.25 Å. The grid was positioned at the coordinates *x* = 34.99, *y* = 15.79, *z* = 14.9 and *x* = 35.05, *y* = 15.89, *z* = 14.9, respectively, to cover the entire active site cavities of DatA and DatA01. Two hundred and fifty docking calculations were performed for each ligand employing the Lamarckian genetic algorithm with the parameters: initial population size of 300, maximum of 30 000 generations, elitism value of 1, mutation rate of 0.02, and cross-over rate of 0.8. The maximum of energy evaluations were set to 10 000 000. The local search was based on the pseudo Solis and Wets algorithm with a maximum of 300 iterations per local search [36]. Energy of the unbound system was estimated as the internal energy of the unbound extended conformation determined from a Lamarckian genetic algorithm search. Final orientations from every docking run were clustered within a clustering tolerance for an r.m.s.d. of 0.5 Å.

### QM calculations

All residues within 12 Å of the bound substrate were simulated in the quantum mechanical calculations. The DatA and DatA01 active site models consisted of 55 amino acids (H41, G42, N43, P44, T45, L49, L68, Y71, L83, Q86, Q107, D108, Y/W109, G110, A111, A112, F113, E132,

P133, V134, I138, L143, S144, P145, F147, L156, F163, V164, F170, L171, L174, F175, P176, F178, F179, A203, I204, L205, A206, G207, P208, N210, L211, P212, V213, T219, L224, G246, F247, L248, I273, H274, F275, V276 and Q277) together with the appropriate substrate molecules. The total charge of the system was  $-2$ . The reaction pathways were mapped using MOPAC 2009 [37] with the MOZYME algorithm [38] and the DRIVER external subroutine [39]. The use of semi-empirical modelling made it possible to perform quantum mechanical calculations despite the relatively large size of the model, which incorporates the entire first shell of the active site and many second shell residues. The  $S_N2$  reaction step was modelled by shortening the distance between the OD1 atom of the nucleophile and the C1 atom of the substrate to which the halogen atom is bound. This distance was reduced by  $0.05 \text{ \AA}$  on each driving step, and the geometry of the system was fully optimized (with the exception of the driven coordinate and the fixed heavy atoms of the protein backbone). All calculations were performed using the AM1 Hamiltonian with Mulliken population analysis for the charge distribution and the BFGS geometry optimization algorithm. The keywords used to control the calculation were: GEO-OK, MMOK, NOINTER, NOXYZ and CHARGE. Data analysis was performed using TRITON, version 2.0b [40–42]. The activation energy of the reaction was approximated as the difference between the heat of formation of the enzyme–substrate and transition state structures, whereas the enthalpy of reaction was calculated as the difference between the heats of formation of the reactants and products. The electrostatic interaction energies ( $E_{el}$ ) were calculated as the sum of all atom–atom interaction energies between each amino acid and the halogen atoms of the substrates and the halide ion, respectively, according to Coulomb's law, using the geometries and partial charges obtained from the MOPAC calculations.

## MD simulations

The lowest energy docking poses in the most populated cluster obtained for the docking of 1-bromohexane with DatA and DatA01 were selected as the starting configurations for subsequent MD simulations. All crystallographic water molecules that did not overlap with the docked ligands were added to the complexes. The system was neutralized by adding sodium cations. Finally, the complexes were immersed in an octahedral box of TIP3P [43] water molecules with a minimum water layer thickness of  $10.0 \text{ \AA}$ . Approximately 7500 water molecules were added to solvate each system. Energy minimization and equilibration were performed using the PMEMD module of the AMBER, version 11 [44] with the ff99SB force field [45]. The equilibration protocol consisted of: (a) 500 steps of steepest descent energy minimization and 500 steps of conjugate gradient minimization of the positions of water molecules and ions,

with the rest of the system being harmonically restrained with a force constant of  $500 \text{ kcal}\cdot\text{mol}^{-1}\cdot\text{\AA}^{-2}$ , (b) three rounds of 1000 steps, involving 500 steepest descent steps followed by 500 steps of conjugate gradient energy minimization, with decreasing constraints on the protein backbone ( $500$ ,  $125$  and  $25 \text{ kcal}\cdot\text{mol}^{-1}\cdot\text{\AA}^{-2}$ ), (c) a final minimization with no constraints ( $0 \text{ kcal}\cdot\text{mol}^{-1}\cdot\text{\AA}^{-2}$ ) applied to the protein backbone, involving 100 steepest descent steps followed by 400 steps of conjugate gradient energy minimization, (d) 2 ns of gradual heating of the whole system from 0 to 300 K over 20 ps using a Langevin thermostat with a temperature coupling constant of  $1.0 \text{ ps}$  in a constant volume periodic box, and (e) an MD production run with a 2-fs time step that was applied to the whole system using the constant pressure periodic boundary conditions. The constant temperature was maintained using the weak-coupling algorithm for 20 ns of the production simulation time, with a temperature coupling constant of  $1.0 \text{ ps}$ . Long-range electrostatic interactions were modelled using the Particle mesh Ewald method with a nonbonded cut-off of  $10 \text{ \AA}$  and the SHAKE algorithm [46]. The coordinates were saved at intervals of  $1 \text{ ps}$ . The resulting trajectories were analyzed using the Ptraj module of AMBER and were visualized using PYMOL, version 1.5 [47] and VMD, version 1.8.6 [48].

## Acknowledgements

The authors would like to thank Professor M. Tanokura (University of Tokyo, Tokyo, Japan) for providing the co-ordinates for the DatA and DatA01 structures before their publication in the Protein Data Bank. MetaCentrum is acknowledged for providing access to computing facilities, supported by the Ministry of Education, Youth and Sports of the Czech Republic (LM2010005). A.G. was supported by SoMoPro programme no. SIGA762 with a financial contribution from the European Commission within the 7th FP (FP/2007–2013) under grant agreement No. 229603 and is co-financed by the South Moravian Region. This work was supported by the Grant Agency of the Czech Republic (P207/12/0775 and P503/12/0572), the Grant Agency of the Czech Academy of Sciences (IAA401630901) and the European Regional Development Fund (CZ.1.05/2.1.00/01.0001).

## References

- 1 Janssen DB, Oppentocht JE & Poelarends GJ (2001) Microbial dehalogenation. *Curr Opin Biotechnol* **12**, 254–258.
- 2 Janssen DB, Dinkla IJT, Poelarends GJ & Terpstra P (2005) Bacterial degradation of xenobiotic compounds: evolution and distribution of novel enzyme activities. *Environ Microbiol* **7**, 1868–1882.

- 3 Kurihara T & Esaki N (2008) Bacterial hydrolytic dehalogenases and related enzymes: occurrences, reaction mechanisms, and applications. *Chem Rec* **8**, 67–74.
- 4 Prokop Z, Sato Y, Brezovsky J, Mozga T, Chaloupkova R, Koudelakova T, Jerabek P, Stepankova V, Natsume R, Van Leeuwen JG *et al.* (2010) Enantioselectivity of haloalkane dehalogenases and its modulation by surface loop engineering. *Angew Chem Int Ed Engl* **49**, 6111–6115.
- 5 Szymański W, Westerbeek A, Janssen DB & Feringa BL (2011) A simple enantioconvergent and chemoenzymatic synthesis of optically active  $\alpha$ -substituted amides. *Angew Chem Int Ed Engl* **50**, 10712–10715.
- 6 Swanson PE (1999) Dehalogenases applied to industrial-scale biocatalysis. *Curr Opin Biotechnol* **10**, 365–369.
- 7 Bidmanova S, Chaloupkova R, Damborsky J & Prokop Z (2010) Development of an enzymatic fiber-optic biosensor for detection of halogenated hydrocarbons. *Anal Bioanal Chem* **398**, 1891–1898.
- 8 Reardon KF, Campbell DW & Müller C (2009) Optical fiber enzymatic biosensor for reagentless measurement of ethylene dibromide. *Eng Life Sci* **9**, 291–297.
- 9 Franken SM, Rozeboom HJ, Kalk KH & Dijkstra BW (1991) Crystal structure of haloalkane dehalogenase: an enzyme to detoxify halogenated alkanes. *EMBO J* **10**, 1297–1302.
- 10 Gehret JJ, Gu L, Geders TW, Brown WC, Gerwick L, Gerwick WH, Sherman DH & Smith JL (2012) Structure and activity of DmmA, a marine haloalkane dehalogenase. *Protein Sci* **21**, 239–248.
- 11 Hesseler M, Bogdanović X, Hidalgo A, Berenguer J, Palm GJ, Hinrichs W & Bornscheuer UT (2011) Cloning, functional expression, biochemical characterization, and structural analysis of a haloalkane dehalogenase from *Plesiocystis pacifica* SIR-1. *Appl Microbiol Biotechnol* **91**, 1049–1060.
- 12 Holmquist M (2000) Alpha/Beta-hydrolase fold enzymes: structures, functions and mechanisms. *Curr Protein Pept Sci* **1**, 209–235.
- 13 Marek J, Védová J, Smatanová IK, Nagata Y, Svensson LA, Newman J, Takagi M & Damborský J (2000) Crystal structure of the haloalkane dehalogenase from *Sphingomonas paucimobilis* UT26. *Biochemistry* **39**, 14082–14086.
- 14 Newman J, Peat TS, Richard R, Kan L, Swanson PE, Affholter JA, Holmes IH, Schindler JF, Unkefer CJ & Terwilliger TC (1999) Haloalkane dehalogenases: structure of a *Rhodococcus* enzyme. *Biochemistry* **38**, 16105–16114.
- 15 Mazumdar PA, Hulecki JC, Cherney MM, Garen CR & James MNG (2008) X-ray crystal structure of *Mycobacterium tuberculosis* haloalkane dehalogenase Rv2579. *Biochim Biophys Acta* **1784**, 351–362.
- 16 Ollis DL, Cheah E, Cygler M, Dijkstra B, Frolow F, Franken SM, Harel M, Remington SJ, Silman I & Schrag J (1992) The alpha/beta hydrolase fold. *Protein Eng* **5**, 197–211.
- 17 Streltsov VA, Prokop Z, Damborský J, Nagata Y, Oakley A & Wilce MCJ (2003) Haloalkane dehalogenase LinB from *Sphingomonas paucimobilis* UT26: X-ray crystallographic studies of dehalogenation of brominated substrates. *Biochemistry* **42**, 10104–10112.
- 18 Verschueren KH, Seljée F, Rozeboom HJ, Kalk KH & Dijkstra BW (1993) Crystallographic analysis of the catalytic mechanism of haloalkane dehalogenase. *Nature* **363**, 693–698.
- 19 Verschueren KH, Kingma J, Rozeboom HJ, Kalk KH, Janssen DB & Dijkstra BW (1993) Crystallographic and fluorescence studies of the interaction of haloalkane dehalogenase with halide ions. Studies with halide compounds reveal a halide binding site in the active site. *Biochemistry* **32**, 9031–9037.
- 20 O'Hagan D & Schmidberger JW (2010) Enzymes that catalyse SN2 reaction mechanisms. *Nat Prod Rep* **27**, 900–918.
- 21 Otyepka M, Banás P, Magistrato A, Carloni P & Damborský J (2008) Second step of hydrolytic dehalogenation in haloalkane dehalogenase investigated by QM/MM methods. *Proteins* **70**, 707–717.
- 22 Prokop Z, Monincová M, Chaloupková R, Klvana M, Nagata Y, Janssen DB & Damborský J (2003) Catalytic mechanism of the haloalkane dehalogenase LinB from *Sphingomonas paucimobilis* UT26. *J Biol Chem* **278**, 45094–45100.
- 23 Bohác M, Nagata Y, Prokop Z, Prokop M, Monincová M, Tsuda M, Koca J & Damborský J (2002) Halide-stabilizing residues of haloalkane dehalogenases studied by quantum mechanic calculations and site-directed mutagenesis. *Biochemistry* **41**, 14272–14280.
- 24 Kennes C, Pries F, Krooshof GH, Bokma E, Kingma J & Janssen DB (1995) Replacement of tryptophan residues in haloalkane dehalogenase reduces halide binding and catalytic activity. *Eur J Biochem* **228**, 403–407.
- 25 Schanstra JP & Janssen DB (1996) Kinetics of halide release of haloalkane dehalogenase: evidence for a slow conformational change. *Biochemistry* **35**, 5624–5632.
- 26 Krooshof GH, Ridder IS, Tepper AW, Vos GJ, Rozeboom HJ, Kalk KH, Dijkstra BW & Janssen DB (1998) Kinetic analysis and X-ray structure of haloalkane dehalogenase with a modified halide-binding site. *Biochemistry* **37**, 15013–15023.
- 27 Chovancova E, Kosinski J, Bujnicki JM & Damborsky J (2007) Phylogenetic analysis of haloalkane dehalogenases. *Proteins* **67**, 305–316.
- 28 Hasan K, Fortova A, Koudelakova T, Chaloupkova R, Ishitsuka M, Nagata Y, Damborsky J & Prokop Z

- (2011) Biochemical characteristics of the novel haloalkane dehalogenase DatA, isolated from the plant pathogen *Agrobacterium tumefaciens* C58. *Appl Environ Microbiol* **77**, 1881–1884.
- 29 Vieille C & Zeikus GJ (2001) Hyperthermophilic enzymes: sources, uses, and molecular mechanisms for thermostability. *Microbiol Mol Biol Rev* **65**, 1–43.
- 30 Hur S, Kahn K & Bruice TC (2003) Comparison of formation of reactive conformers for the SN<sub>2</sub> displacements by CH<sub>3</sub>CO<sub>2</sub><sup>-</sup> in water and by Asp124-CO<sub>2</sub><sup>-</sup> in a haloalkane dehalogenase. *Proc Natl Acad Sci USA* **100**, 2215–2219.
- 31 Koudelakova T, Chovancova E, Brezovsky J, Monincova M, Fortova A, Jarkovsky J & Damborsky J (2011) Substrate specificity of haloalkane dehalogenases. *Biochem J* **435**, 345–354.
- 32 Iwasaki I, Utsumi S & Ozawa T (1952) New colorimetric determination of chloride using mercuric thiocyanate and ferric ion. *Bull Chem Soc Jpn* **25**, 226.
- 33 Gordon JC, Myers JB, Folta T, Shoja V, Heath LS & Onufriev A (2005) H<sup>++</sup>: a server for estimating pK<sub>a</sub>s and adding missing hydrogens to macromolecules. *Nucleic Acids Res* **33**, W368–W371.
- 34 Morris GM, Goodsell DS, Halliday RS, Huey R, Hart WE, Belew RK & Olson AJ (1998) Automated docking using a Lamarckian genetic algorithm and an empirical binding free energy function. *J Comp Chem* **19**, 1639–1662.
- 35 Sanner MF (1999) Python: a programming language for software integration and development. *J Mol Graph Model* **17**, 57–61.
- 36 Solis FJ & Wets RJ-B (1981) Minimization by random search techniques. *Math Oper Res* **6**, 19–30.
- 37 Stewart JJP (2008) MOPAC2009 Stewart Computational Chemistry. Colorado Springs, CO, USA.
- 38 Stewart JJP (1996) Application of localized molecular orbitals to the solution of semiempirical self-consistent field equations. *Int J Quantum Chem* **58**, 133–146.
- 39 Černohorský M, Kutý M & Koca J (1997) A multidimensional driver for quantum chemistry program MOPAC. *Comp & Chem* **21**, 35–44.
- 40 Prokop M, Adam J, Kríz Z, Wimmerová M & Koca J (2008) TRITON: a graphical tool for ligand-binding protein engineering. *Bioinformatics* **24**, 1955–1956.
- 41 Prokop M, Damborský J & Koca J (2000) TRITON: in silico construction of protein mutants and prediction of their activities. *Bioinformatics* **16**, 845–846.
- 42 Damborský J, Prokop M & Koca J (2001) TRITON: graphic software for rational engineering of enzymes. *Trends Biochem Sci* **26**, 71–73.
- 43 Jorgensen WL, Chandrasekhar J, Madura JD, Impey RW & Klein ML (1983) Comparison of simple potential functions for simulating liquid water. *Journal of Chemical Physics* **79**, 926–935.
- 44 Case DA, Darden TA, Cheatham TE, Simmerling CL, Wang J, Duke RE, Luo R, Crowley M, Walker RC, Zhang W *et al.* (2010) Amber 11. University of California, San Francisco.
- 45 Hornak V, Abel R, Okur A, Strockbine B, Roitberg A & Simmerling C (2006) Comparison of multiple Amber force fields and development of improved protein backbone parameters. *Proteins* **65**, 712–725.
- 46 Ryckaert J-P, Ciccotti G & Berendsen HJ (1977) Numerical integration of the cartesian equations of motion of a system with constraints: molecular dynamics of n-alkanes. *J Comput Phys* **23**, 327–341.
- 47 Schrödinger L (2010) The PyMOL Molecular Graphics System, Version 1.5.
- 48 Humphrey W, Dalke A & Schulten K (1996) VMD: visual molecular dynamics. *J Mol Graph* **14**, 27–28.

## Supporting information

Additional supporting information may be found in the online version of this article at the publisher's web site:

**Fig. S1.** CD spectra of DatA and DatA01.

**Fig. S2.** Comparison of the reaction energy profiles obtained from QM calculations.

**Fig. S3.** Comparison of the halide ion stabilization by the active site residues obtained from QM calculations.

**Table S1.** Geometries of enzyme–substrate complexes selected from MD snapshots as inputs for QM calculations.

**Table S2.** Activation energies ( $E_a$ ) and enthalpies ( $\Delta H$ ) for the hydrolysis of various substrates calculated from the reaction profiles.